jmr&t
Journal of Materials Research and Technology
www.jmrt.com.br

Short Communication

Parametric study of the ductile damage by the Gurson–Tvergaard–Needleman model of structures in carbon steel A48-AP

Abdelkader Slimane[a,*], *Benattou Bouchouicha*[a], *Mohamed Benguediab*[a], *Sid-Ahmed Slimane*[b]

[a] *Laboratory of Materials and Reactive Systems LMSR, Department of Mechanical Engineering, University Djilali Liabes, Sidi Bel Abbes, Algeria*

[b] *Laboratory of Applied Mechanics, Department of Mechanical Engineering, University of Science and Technology Mohamed Boudiaf, Oran, El-Mnaouer, Algeria*

ARTICLE INFO

Article history:
Received 27 May 2014
Accepted 20 December 2014
Available online 7 February 2015

Keywords:
GTN model
Ductile damage
Nucleation
Damage of materials

ABSTRACT

This part of study is devoted to the numerical simulation of axisymmetric notched specimens in order to study the phenomenon of nucleation by Gurson–Tvergaard–Needleman model (GTN). The numerical simulations were performed to describe the damage of the materials using GTN model, which involves the stress triaxiality. The specimens chosen are somewhat axisymmetric notched (AN): hence, this choice was motivated by the symmetry of these specimens, and also by the existence of notches that make them interesting in the case of fracture mechanics.

1. Introduction

Ductile tearing is the failure mode that particularly concerns us in this work. It occurs when a structure is subjected to an increasing monotonic loading, wherein the constituent material can endure important plastic deformations.

A48-AP steel was chosen for this study because of our works [1] that has already been made on this steel; therefore, its behavior and mechanical properties are well known, such as the yield strength, Young's modulus and Poisson's ratio. These data allow to reproduce the real behavior of this material.

A parametric analysis was performed to elucidate the influence of the nucleation parameters and evolution of the responses of axisymmetric notched specimens based on these two parameters. The values of the other parameters were fixed according to the most used values in the literature for this steel such q_1 to 1.5 and q_2 to 1. The notch locates the deformations in the middle of the specimen during the loading and allows

* *Corresponding author.*
E-mail: slimane.aek@hotmail.com (A. Slimane).

http://dx.doi.org/10.1016/j.jmrt.2014.12.011

Nomenclature

σ_0	yield strength of the material
$\sum_m = \sum_{kk}/3$	the hydrostatic stress (mean stress)
$\sum_{eq}$	equivalent stress of Von Mises
$q1$, $q2$, $q3$	material parameters
f^*	function f defined as following
f_u^*	ultimate value of $f = 1/q_1$
f_F	void volume fraction at the final fracture
f_c	threshold value which indicates the onset of coalescence
Φ	current diameter of the minimum section of the specimen
$\Delta\Phi$	reduction of the diameter
Le	mesh size
f_n	void volume fraction nucleated at the level of inclusions
E	Young's modulus
ν	Poisson's ratio
σ_e	yield strength of the material
f_0	initial void volume fraction
ε_n	average strain at onset of nucleation cavities
S_n	corresponding standard deviation

practically to evaluate the mechanical quantities in this level, such as the displacement at the bottom of the notch.

2. Gurson–Tvergaard–Needleman model (GTN)

2.1. Gurson criterion

Gurson [2] considers a hollow sphere with a spherical cavity shown in Fig. 1, the matrix of rigid-perfectly plastic behavior obeying the plasticity criterion of Von Mises yield strength σ_0, subjected to conditions of uniform and homogeneous strain rate, applied to the outer edge.

The approached macroscopic criterion represents the plastic potential Φ with the function of the flow surface depending on the macroscopic stress and the void volume fraction randomly distributed [4]:

$$\Phi(\Sigma, f, \sigma_0) = \frac{\Sigma_{eq}^2}{\sigma_0^2} + 2f \cdot \coh\left(\frac{3}{2}\frac{\Sigma_m}{\sigma_0}\right) - 1 - f^2 = 0 \quad (1)$$

with σ_0, yield strength of the material; $\Sigma_m = \Sigma_{kk}/3$, hydrostatic stress (mean stress); $\sum_{eq}$, equivalent stress of Von Mises.

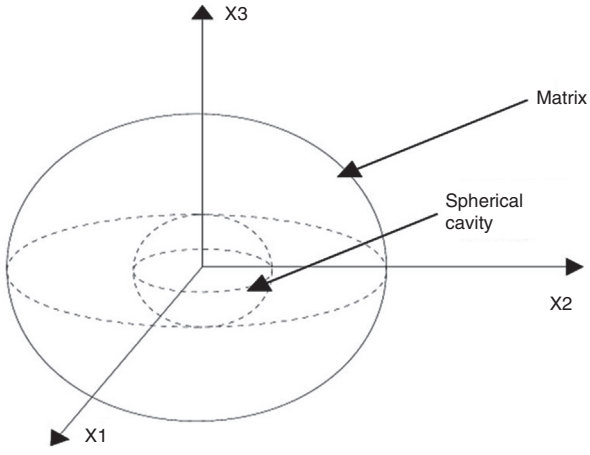

Fig. 1 – Model of the hollow sphere under conditions of uniform deformation rate at the edge [3].

2.2. Gurson–Tvergaard criterion (G–T)

Gurson model gives satisfactory approximations for high of stress triaxiality, but in the case of low rates of stress triaxiality, the model overestimates the failure strain (ductility). Tvergaard [5] proposes to introduce three parameters (q_1, q_2 and q_3) to address this problem by taking into account the interaction between cavities.

Then Tvergaard proposes the following threshold function:

$$\Phi(\Sigma, \bar{\sigma}, f) = \frac{\Sigma_{eq}^2}{\bar{\sigma}^2} + 2q_1 f \cdot \cosh\left(\frac{3}{2}q_2\frac{\Sigma_m}{\bar{\sigma}}\right) - 1 - q_3 f^2 = 0 \quad (2)$$

Several values of the parameters q_1, q_2 and q_3 have been proposed by the authors and experiments are carried out to approximate the real behavior of structures. The values most encountered in the literature are: $q_1 = 1.5$, $q_2 = 1$, $q_3 = {q_1}^2$

2.3. Gurson–Tvergaard–Needleman criterion (GTN)

According to experiments, it turns out that the Gurson–Tvergaard (GT) model [5] does not account for the rapid loss of material stiffness and does not adequately describe the effects of voids coalescence, because it does not constitute a failure criterion. From the experimental observations, the coalescence can be supposed effective when the void volume fraction reaches a critical value f_c, which indicates the onset of coalescence.

Needleman has modified the previous criterion (GT model) to take into account the sharp drop in stiffness of the material by the following threshold function (GTN model) [6,7]:

$$\Phi(\Sigma, \bar{\sigma}, f) = \frac{\Sigma_{eq}^2}{\bar{\sigma}^2} + 2q_1 f^* \cdot \cosh\left(\frac{3}{2}q_2\frac{\Sigma_m}{\bar{\sigma}}\right) - 1 - (q_1 f^*)^2 = 0 \quad (3)$$

where f^* is a function of f defined as following:

$$f^* = \begin{cases} f & \text{pour } f \le f_c \\ f + \delta(f - f_c) & \text{pour } f > f_c \end{cases} \quad (4)$$

with:

$$\delta = \frac{f_u^* - f_c}{f_F - f_c} \quad (5)$$

f_u^* is the ultimate value of $f = 1/q_1$, f_F is the volume fraction of the void at the final fracture, f_c is a threshold value, which indicates the onset of coalescence.

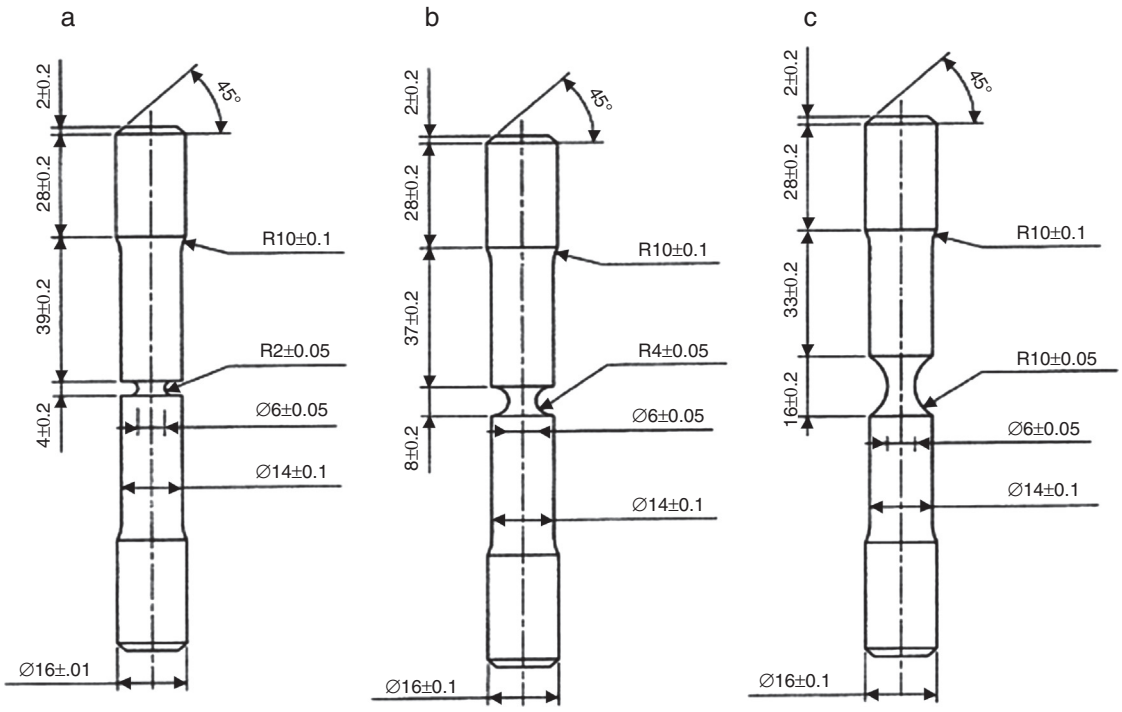

Fig. 2 – Specimen geometry (a) AN2, (b) AN4 and (c) AN10 [8].

3. Choice of specimens

The choice of axisymmetric notched specimens (AN) was motivated by several advantages. First of all, unlike the case of smooth tensile specimens where the phenomenon of necking does not occur necessarily in the middle of the specimens, necking of axisymmetric notched specimens (AN) develops at the notch. By varying on the radius of the notch (therefore the rate of stress triaxiality).

In addition, the axisymmetric geometry of the specimen allows a two-dimensional modeling into axisymmetric mode by a finite elements calculation for an isotropic material.

It should be noted that the modeling in axisymmetric mode is under assumption of isotropy of the material, without this assumption, the modeling will be done in three-dimensional elements.

3.1. *Geometry of specimens*

The specimen geometry is given in Fig. 2 with dimensions expressed in millimeters. These specimens are AN2, AN4 and AN10 with notch radius of 2, 4 and 10 mm, respectively, and they have a diameter of 6 mm in the bottom of notch. We note that Φ is the current diameter of the minimum section of the specimen and $\Delta\Phi = \Phi_0 - \Phi$ is the diameter reduction.

The specimens AN2, AN4 and AN10 are respectively called strongly, moderately and weakly notched, they allow to develop in the center of each specimen a relatively stable triaxiality from an average strain.

4. Mesh and boundary conditions

By symmetry, only a quarter of the meridian plane is modeled in axisymmetric mode (Fig. 3). It is seen that the specimen has two planes of symmetry, and then the sides of the symmetry planes of the specimen will be blocked (by displacement) in the perpendicular sense to the symmetry planes.

This axisymmetric modeling saves computing time compared to 3D modeling, which requires a longer calculation

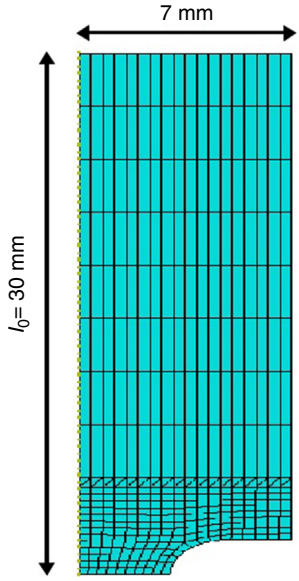

Fig. 3 – Dimensions and mesh of the selected specimen.

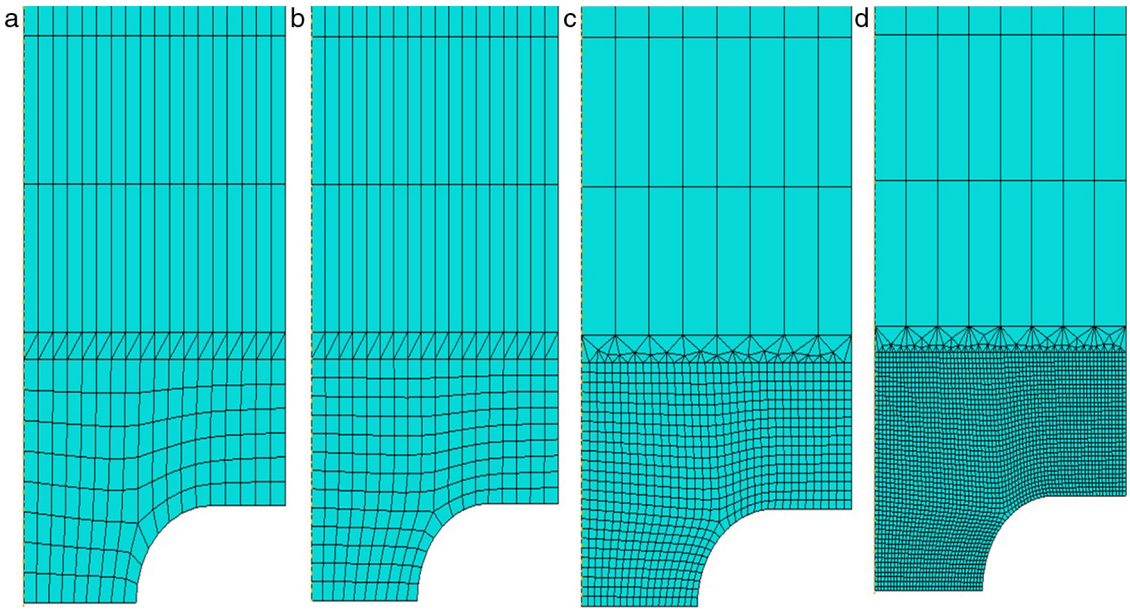

Fig. 4 – Different meshes used. (a) Mesh M_1 (Le = 0.4), (b) Mesh M_2 (Le = 0.2), (c) Mesh M_3 (Le = 0.1), (d) Mesh M_4 (Le = 0.05).

time, but the axisymmetric modeling assumes that the mechanical parameters remain constant in the direction of θ relative to the axis of the specimen; this is not inevitably correct in a 3D modeling, which is more representative of reality.

The mesh is composed of quadratic axisymmetric elements with 8 nodes, the first mesh is used to perform the first calculation and visualize the first results, which will not be necessarily accurate, but can give us indications on the computation time, the progress of the calculation program and zones of high gradient to refine a little more the mesh in these zones.

For the choice of the mesh (the mesh size), it must be done according to the nature of the simulated material, the size of its grains, its defects, its imperfections and also the evolution of these imperfections during loading.

We shall proceed to the mesh refining near the notch because in this zone the gradient of strain and stress is intense, unlike the upper part of the specimen, The refining of the meshing will not be important as long as we are interested in the zone near the notch, which saves a little more of computing time.

The boundary conditions and loading are the same whatever the specimen:

- Blocking the displacement along the *x*-axis for adjacent nodes to the *Y*-axis.
- Blocking the displacements along the *Y*-axis for the adjacent nodes to the *x*-axis.
- Loading imposed on the *Y*-axis for the nodes located at the upper part of the specimen.

5. Mesh sensitivity

Fig. 4 shows the four meshes used from the coarsest M_1 to the finest M_4, the size of the elements at the notched zone is divided by 2 by passing from the mesh M_1 to M_2, from M_2 to M_3 and from M_3 to M_4. The mesh of the upper part of the specimen is not refined, because this part is not subject to strong variations on the one hand and on the other hand, our study concerns the port near the notch.

This mesh allows us to avoid making a longer calculation time, compared with a refined mesh over the whole surface of the specimen; even if the difference of the elements size between the upper part and the lower part of the specimen is important, it does not affect the precision of our calculations, seen that the mechanical fields, which we are particularly interested, are located in the lower part of the specimen.

The following figures show the simulation results obtained on the four meshes used:

Fig. 5 represents the load-diameter reduction curve for each case of mesh for an elastoplastic behavior, and this figure shows that the damage affects the material as soon as the yield strength is exceeded; this is resulted in degradation of

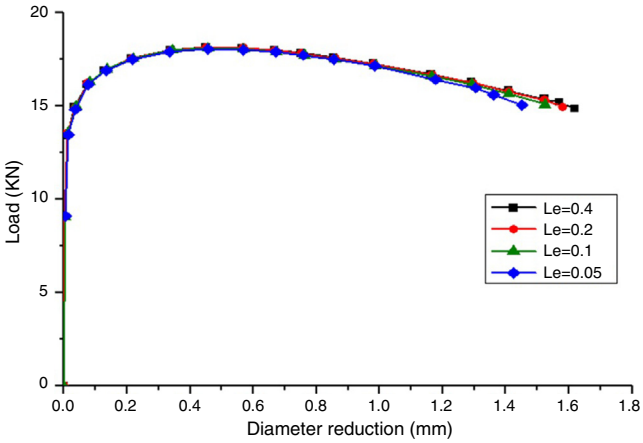

Fig. 5 – Influence of the mesh on the load-diameter reduction curve.

the load just after the elastic phase and before the crack initiation. It is noted that this degradation is progressive and linear up to the point of crack initiation.

Also, this figure shows that the elastoplastic part is very insensitive to the mesh because the curves are practically identical in both cases; contrary to the fracture part, the curves are not identical because of the difference of initiation point for every mesh. A finer mesh than another precipitates the voids initiation.

The speed of degradation of the load remains relatively the same for the four cases of meshes.

6. Effect of f_n

The f_n parameter represents the void volume fraction nucleated at the level of inclusions, we conducted many models with the mesh M_3 and by varying the f_n parameter from 0.001 to 0.006 (Table 1), all other parameters of this case are kept fixed.

Several values are assigned to f_n parameter to see its influence on the system response. The responses obtained are given in the presented figure, which represents the evolution of the equivalent stress according to the nominal strain of the specimen.

The figure shows that the elastic–plastic part is completely insensitive to variations of f_n; the curves at this level are totally confused. The difference lies in the fraction part at the point of void initiation and the falling speed of the load.

It is found that the increase of the value of f_n precipitates the voids initiation and increases the falling speed of the load (in the fracture part).f_n parameter is representative of the volume fraction when new void initiation happens during deformation [9], as well as the increase of its value is reflected in the increase of the number of cavities presented in the matrix. As can be found from Fig. 6, the f_n value influences the fracture position of the equivalent stress–nominal strain curve of notched specimens. Higher f_n values can lead to earlier failure of the specimen while the slope of all the curves after fracture initiation is constant; therefore, its mechanical properties are affected and weakened, that is resulted in the rapid degradation of the load and voids initiation for low loads.

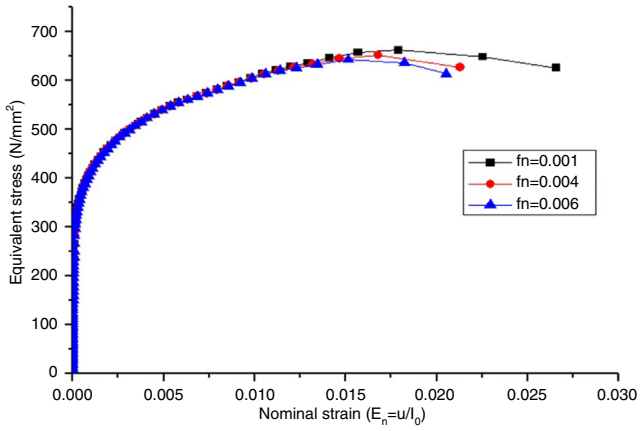

Fig. 6 – Influence of f_n on the behavior of the specimen.

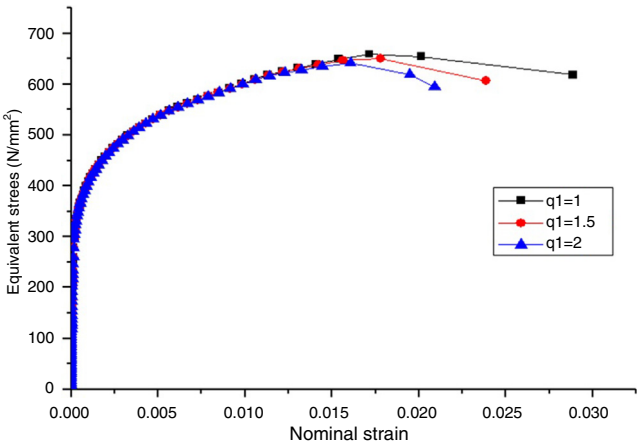

Fig. 7 – Influence of q_1.

7. Effect of q_i

The effect of the void volume fraction of the Gurson model depends on the definition of three parameters q_i ($i = 1, 2$ and 3) introduced by Tvergaard [10].

Figs. 7 and 8 show the effect of q_i using an axisymmetric notched specimen. The growth of q_i increases the effect of the void volume fraction, which results in more severe decreases in tensile strength.

Relatively important values of q_i up to 2 are also included for comparison where the influence of q_2 is more important than the effect of q_1 in the fracture part, especially on the point of void initiation and the falling speed of the load.

The plastic limit is encountered for reduced stress conditions when $q_1 > 1$. Higher values of parameter q_1 decrease the strength of the GTN material [11]. The equivalent stress–nominal strain curve is influenced by parameter q_1 modifying the stress carrying capacity, which reveal the softening due to void growth dominating over hardening properties of the matrix material.

For higher values of q_1 the stronger softening of the material is observed (Fig. 7). The value of $q_1 = 1.5$ was proposed by Tvergaard [12,13] as optimal to model

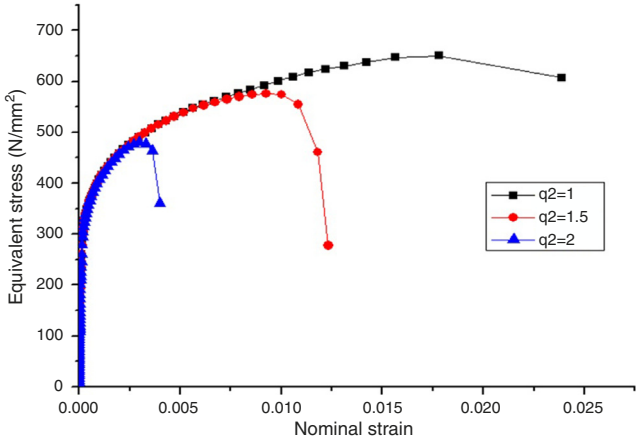

Fig. 8 – Influence of q_2.

Table 1 – Parameters of the GTN damage model.

E (GPa)	ν	σ_e (MPa)	q_1	q_2	q_3	f_0	f_n	ε_n	S_n
183	0.3	325	1.5	1	$(q_1)^2 = 2.25$	1e−5	0.001–0.004–0.006	0.3	0.1

numerically the localization of plastic deformations effect and fracture phenomena for many porous solids, including metals.

The second Tvergaard's parameter q_2 modifies first invariant of the stress state Σ_{kk} being a function of the hydro-static component $\Sigma_m = \Sigma_{kk}/3$. For high values of q_2 the yield limit is strongly reduced. According to Tvergaard's results [14] the suggested value was determined as $q_2 = 1$. High values of q_2 lead to the strong softening due to the void growth, revealing the annihilation of the strain hardening properties of the matrix material (Fig. 8). Then overall strength properties of the porous GTN material are reduced.

As concluded, typical and suggested values of Tvergaard's parameters for steel grades were established as $q_1 = 1.5$, $q_2 = 1$ and $q_3 = q_1{}^2 = 2.25$. The values of q_1 and q_2 parameters are related to the elastic–plastic properties of the material [15], defined by strain hardening exponent and yield stress to modulus of elasticity E ratio.

8. Conclusion

The choice of a finite element model with axisymmetric elements was motivated both by the necking produced in the middle of specimens and the short computing time compared to the three-dimensional modeling.

The choice of the mesh was justified by the nature of its material, its properties, as well as by the results obtained, and the size of the element should be sufficiently large relative to the material heterogeneities to have a homogeneous distribution of these defects on the elements.

On the other hand, the size of the elements must not exceed certain dimensions that distort the results and give bad distributions of fields of mechanical quantities.

The parametric study showed the influence of the mesh and q_i and f_n parameters on the load-diameter reduction and equivalent stress–nominal strain curves. It has been found that refining of the mesh has a very little influence on the elastoplastic part; contrariwise, it affects in a significant way on the point of void initiation.

The variation in the f_n parameter has no influence on the elastoplastic part of the material, but plays a more important role in the fracture part especially on the point of void initiation and the falling speed of the load.

Tvergaard's parameters affected significantly the void growth, which corresponds to the response of A48-AP steel [1] and the failure moment was observed visible earlier due to the much rapid and intensive void growth.

Conflict of interest

The authors declare no conflicts of interest.

Acknowledgement

I want to thank all the authors for their insightful comments and suggestions.

REFERENCES

[1] Slimane A, Bouchouicha B, Benguediab M, Slimane S. Contribution to the study of fatigue and rupture of welded structures in carbon steel-A48 AP: experimental and numerical study. In: Transactions of the Indian Institute of Metals; 2014.
[2] Gurson A. Continuum theory of ductile rupture by void nucleation and growth: part 1. Yield criteria and flow rules for porous ductile media. J Eng Mater Technol 1977;99: 2–15.
[3] Bellache F. Etude de la rupture ductile des matériaux (modèle GTN). Université des Sciences et Technologies de Lille; 2007.
[4] Naït Abdelaziz M. Contribution à l'étude de la déchirure des matériaux par approche globale et approche locale de la mécanique de la rupture. Habilitation à Diriger des Recherches. Université des Sciences et Technologies de Lille; May 1997.
[5] Corigliano A, Mariani S, Orsatti B. Identification of Gurson–Tvergaard material model parameters via Kalman filtering technique: I. Theory. Int J Plast 2000;104: 349–73.
[6] Pardoen T, Doghri T, Delannay F. Experimental and numerical comparison of void growth models and void coalescence criteria for the prediction of ductile fracture in copper bars. Acta Mater 1998;46:541–52.
[7] Kossakowski P. The simulation of the plastic range for structural steels under multiaxial state of stress basing on the Gurson–Tvergaard–Needleman model [Symulacja plastycznego zakresu pracy stali konstrukcyjnych w złozonym stanie naprezen w oparciu o *model Gursona-Tvergaarda-Needlemana*]. Przeglad Budowlany 2012;3:43–9 [in Polish].
[8] Wilsus J [Thèse de doctorat] Etude expérimentale et numérique de la déchirure ductile basée sur des approches locales en mécanique de la rupture. Université des Sciences et Technologies de Lille; 1999.
[9] Kossakowski P. An analysis of the load-carrying capacity of elements subjected to complex stress states with a focus on the microstructural failure. Arch Civil Mech Eng 2010;10:15–39.
[10] Tvergaard V. On localization in ductile materials containing spherical voids. Int J Fract 1982;18:237–52.
[11] Kossakowski PG, Trampczynski W. Numerical simulation of S235JR steel failure with consideration of the influence of microstructural damages [Numeryczna symulacja zniszczenia stali S235JR z uwzglednieniem wpływu uszkodzen mikrostrukturalnych]. Przeglad Mechaniczny 2011;4:15–22 [in Polish].
[12] Tvergaard V. Influence of voids on shear band instabilities under plane strain condition. Int J Fract 1981;17:389–407.

[13] Xia L, Shih CF. Ductile crack growth – II. Void nucleation and geometry effects on macroscopic fracture behavior. J Mech Phys Solids 1995;43:1953–81.
[14] Tvergaard V. Material failure by void growth to coalescence. Adv Appl Mech 1989;27:83–151.
[15] Kossakowski PG. Simulation of ductile fracture of S235JR steel using computational cells with microstructurally-based length scales. J Theor Appl Mech 2012;50: 589–607.